

## Thiophene, Benzothiadiazole Copolymers: Synthesis, Optoelectronic Properties and Electrical Characterization for Photovoltaic Application

Ashraf A El-Shehawey<sup>1\*</sup>, Nabiha I Abdo<sup>2</sup>, Ahmed A El-Barbary<sup>3</sup>, Jin Woo Choi<sup>4</sup>, Hamdy S El-Sheshtawy<sup>1</sup> and Jae-Suk Lee<sup>4\*</sup>

<sup>1</sup>Department of Chemistry, Faculty of Science, Kafrelsheikh University, Egypt

<sup>2</sup>Higher Institute of Engineering and Technology, Alexandria, Egypt

<sup>3</sup>Department of Chemistry, Faculty of Science, Tanta University, Egypt

<sup>4</sup>School of Material Science and Engineering, The Grubbs Center for Polymers and Catalysis and Research Institute for Solar and Sustainable Energy, Gwangju Institute of Science and Technology, Republic of Korea

\*Corresponding author: Ashraf A El-Shehawey, Faculty of Science, Department of Chemistry, Kafrelsheikh University, Egypt, Tel: 0473-214998; E-mail: [elshehawey65@yahoo.com](mailto:elshehawey65@yahoo.com)

Jae-Suk Lee, School of Material Science and Engineering, The Grubbs Center for Polymers and Catalysis and Research Institute for Solar and Sustainable Energy, Gwangju Institute of Science and Technology, Gwangju, Republic of Korea, Tel: 8262-7152306; Fax: 8262-7152304; E-mail: [jslee@gist.ac.kr](mailto:jslee@gist.ac.kr)

(H. S. El-Sheshtawy contributed only in a part of discussing the theoretical calculations)

Received date: December 30, 2017; Accepted date: January 30, 2018; Published date: February 5, 2018

Copyright: © 2018 El-Shehawey AA, et al. This is an open-access article distributed under the terms of the Creative Commons Attribution License, which permits unrestricted use, distribution, and reproduction in any medium, provided the original author and source are credited.

### Abstract

Several donor-acceptor  $\pi$ -conjugated copolymers were synthesized by combining 4,7-bis(3,3',4,4'-hexylthiophene-2-yl)benzo[c][2,1,3]thiadiazoles (HT-BzT-HT) with different donor segments, including thiophene, 2,2'-bithiophene, thieno[3,2-b]thiophene and dithieno[3,2-b;2',3'-d]thiophene via Stille cross-coupling methodology, under microwave irradiation. All copolymers exhibited good solubility in most common organic solvents and showed high thermal stabilities. The revealed relationships between the molecular structure and optoelectronic properties were discussed. Each of DFT/TDDFT theoretical calculations and experimental measurements showed that moving the hexyl side chains from 3,3'- to 4,4'- positions in the thiophene rings of HT-BzT-HT units leads to a decrease both optical and electrochemical band gaps. Electrochemical characterization showed that the estimated HOMO and LUMO energy levels are in the range of -5.18 eV to -5.60 eV and -3.25 to -3.53 eV, respectively. The PCE of 1.91% was obtained from P10/PC<sub>60</sub>BM based device with  $V_{oc}$  of 0.64 V,  $J_{sc}$  of 5.68 mA/cm<sup>2</sup> and fill factor of 64%.

**Keywords:**  $\pi$ -Conjugated copolymers; Solar cell; Donor/acceptor; Benzothiadiazole; Cross-coupling; DFT and TDDFT calculations

### Introduction

Over the past two decades,  $\pi$ -conjugated organic and polymeric materials have attracted significant attention for organic electronics [1-3]. Particularly, polymeric materials are promising for organic photovoltaic cells (OPVs) applications due to several unique properties such as flexibility, solution processability, large area applicability and absorption tenability [2-5]. In an effort to improve the PCE, it has been generally proven that the short circuit current ( $J_{sc}$ ) should be maximized through efficient and wide absorption range among the solar spectra. To increase absorptivity of polymeric semiconducting materials, a popular strategy is conjugated polymers structure with composed of alternating electron-donating (D) and electron-accepting (A) moieties [6-11]. The intramolecular charge transfer (ICT) mechanism within the D/A structure increase the effective resonance length of the  $\pi$ -electrons. However, the absorption peaks and coefficients seems related to the selectivity of the electron donor and acceptor moieties which leads to efficient photon harvest and exciton dissociation [12,13]. Recently, the D/A structure approach has produced a number of useful materials capable of exhibiting recording performances to over than 10% in photovoltaic (PVCs) [3,4,14-20]. Thus, the careful design and selection of the donor and acceptor molecular units for tuning HOMO and LUMO energy levels (i.e., band gaps,  $E_g$ ) of D/A structure polymer remains a challenge [4,21-23]. It is

worth to mention that computational molecular modeling of conjugated polymers using density functional theory (DFT) method at B3LYP level have been proved particularly able to accurately predict the energetic structures and understanding the electronic structure/properties relationships for electronic applications. However, this methodology has been used to estimate the values for each of HOMO and  $E_g$  compared to the obtained experimental values [24,25].

In recent years, OPVs of alternating 2,1,3-benzothiadiazole D/A based copolymers showed impressive PCEs due to the proper electronic characteristic and efficient ICT [12-14,17,18,26,27]. However, fused thiophene of 2,1,3-benzothiadiazole are promising candidates since their backbone structures could provide a rigid and planar  $\pi$ -conjugation system. Highly ordered  $\pi$ - $\pi$  stacking property can be produced due to their rigidity and planarity which intrinsically affords smaller band gaps. Moreover, fused arenes can generally impart quinoid character to the oligomer/polymer and thus lower the band gap relative to, e.g. simple polythiophenes where twisting from planarity can easily disrupt conjugation [12-14,28,29].

We suggest herien the synthetic pathways and characterization of several  $\pi$ -conjugated copolymers on the basis of the aforementioned considerations as well as in continuation to our interest in the several  $\pi$ -conjugated polymers and small molecules for optoelectronic applications [30-37]. 4,7-Bis(3,3'/4,4'-hexylthiophene-2-yl)benzo[c][2,1,3]thiadiazole (HT-BzT-HT) comonomers along with other donors were synthesized via palladium-catalyzed Stille cross-coupling method under microwave reaction conditions. The positioning effect of hexyl

side chains in thiophene rings of HT-BzT-HT on each of the photophysical and electrochemical properties have been studied. The synthesized polymer showed proper HOMO and LUMO level which expected in computational study. Bulk heterojunction solar cell made from copolymer P10/PC<sub>60</sub>BM blend has a power conversion efficiency of 1.91% under 100 mW/cm<sup>2</sup> AM 1.5 sunlight.

## Materials and Methods

### General

All manipulations and reactions involving air-sensitive reagents were performed under a dry oxygen-free nitrogen atmosphere. All reagents and solvents were obtained from commercial sources and dried using standard procedures before use. <sup>1</sup>H- and <sup>13</sup>C-NMR spectra were measured on a Varian spectrometer (400 MHz for <sup>1</sup>H and 100 MHz for <sup>13</sup>C) in CDCl<sub>3</sub> at 25°C with TMS as the internal standard and chemical shifts were recorded in ppm units. The coupling constants (J) are given in Hz. Flash column chromatography was performed with Merck silica gel 60 (particle size 230-400 mesh ASTM). The UV-Vis absorption spectra were obtained using a Varian Cary UV-Vis-NIR-5000 spectrophotometer on the pure polymer samples. Thermal degradation temperature was measured using thermogravimetric analysis (TGA-TA instrument Q-50) under nitrogen atmosphere. Differential scanning calorimetry (DSC) was performed on a TA instrument (DSC-TA instrument Q-20) under nitrogen atmosphere at a heating rate of 10°C/min. Cyclic voltammetry (CV) measurements were performed on B-class solar simulator: Potentiostat/Galvanostat (SP-150 OMA company); The supporting electrolyte was tetrabutylammoniumhexafluorophosphate (TBAPF<sub>6</sub>) in acetonitrile (0.1 M) at a scan rate of 50 mV s<sup>-1</sup>. A three-electrode cell was used; A Pt wire and silver/silver chloride (Ag in 0.1 M KCl) were used as the counter and reference electrodes, respectively. The HOMO and LUMO energy levels of all copolymers were calculated from the onset of the oxidation and reduction potentials (E<sub>ox</sub> and E<sub>re</sub>, respectively), according to the empirical formulas [38,39]: E<sub>HOMO</sub> = -(E<sub>ox</sub> + 4.72) eV and E<sub>LUMO</sub> = -(E<sub>re</sub> + 4.72) eV. The polymer films for electrochemical measurements were spin coated from a polymer-chlorobenzene solution on ITO glass slides, ca. 10 mg/mL. XRD experiments were performed on a Bruker D8 advanced model diffractometer with CuK-α radiation (λ = 1.542 Å) at a generator voltage of 40 kV and a current of 40 mA. The TEM results were obtained on a JEOL 4000FX microscope operated at 300 kV. GPC analysis was carried with a Shimadzu (LC-20A Prominence Series) instrument; Chloroform was used as a carrier solvent (flow rate: 1 mL/min, at 30°C) and calibration curves were made with standard polystyrene samples. Microwave assisted polymerizations were performed in a focused microwave synthesis system<sup>CEM</sup> (Discover S-Class System).

### Device fabrication

The ITO coated glass was cleaned in ultrasonic bath with DI water, acetone and isopropyl alcohol for 15 min. Sonication in isopropyl alcohol decrease surface energy of the substrate and increase its wetting properties and then cleaned with UV-ozone for 15 min. UV-ozone cleaning further changes the surface energy by increasing density of oxygen bonds on the surface. Highly conducting poly(3,4-ethylenedioxythiophene):poly(styrene sulfonate) (PEDOT:PSS, Baytron P, AL4083) was spin coated at 5000 rpm for 40 s and backed at 120°C for 10 min. The active layer contained a blend of copolymers as electron donor and PC60BM as electron acceptor, which was prepared

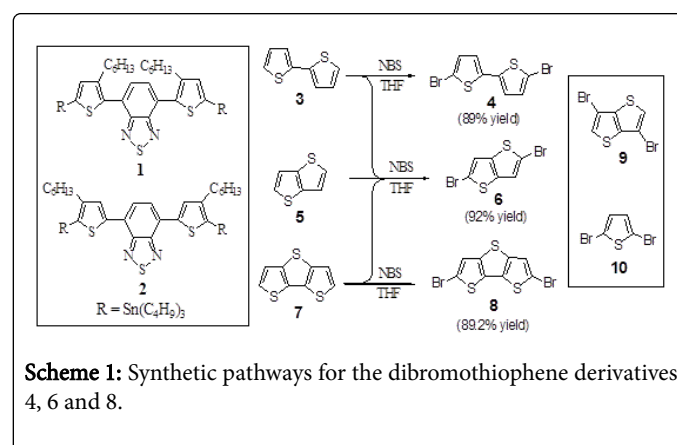
from a 1:1 by weight solution (12 mg/mL) in chlorobenzene (CB), then spin-coating the blend from solution at 2000 rpm. Its thickness was measured using surface profiler (NanoMap 500 LS). Al (100 nm) cathode was thermally evaporated through shadow mask via thermal evaporation in vacuum (<5 × 10<sup>-7</sup> torr). Thermal annealing was carried out by directly placing the device on a hotplate, in a glove-box for 10 min at 90°C under N<sub>2</sub> ambient. Current-voltage (I-V) characteristics were recorded using Keithley 2420 SourceMeter under illumination of an AM 1.5 G (AM=Air Mass) solar simulator with an intensity 100 mW/cm<sup>2</sup> (Oriol<sup>+</sup>, Sol3A<sup>TM</sup>). All devices were fabricated and tested in oxygen and moisture free nitrogen ambient inside the glove-box.

### Theoretical calculations

All theoretical calculations were performed using Gaussian 03 program [24,25,40]. The polymers were optimized at B3LYP/6-311G++(d,p) level of theory. In order to verify the stationary points on the potential energy surface, analytical frequency calculations were performed at the level of theory. TD-DFT were performed on the optimized structures to calculate the excitation energies at B3LYP/6-311++G(d,p) level of theory.

### Synthesis of 5,5'-dibromo-2,2'-bithiophene 4, 2,5-dibromothieno[3,2-b]thiophene 6, and 5,5'-dibromodithieno[3,2-b;2',3'-d]thiophene 8 (General procedure)

N-Bromosuccinimide (NBS) (3.55 g, 20.0 mmol) was added in one portion to an ice-cold solution of thiophene derivative (3, 5 or 7; 10.0 mmol) in dry THF (25 mL). After having been stirred for 30 min at 0°C, the reaction mixture was stirred overnight at room temperature, followed by quenching with saturated aqueous NH<sub>4</sub>Cl. The reaction mixture was extracted with ethyl acetate and the collected organic layers were dried with anhydrous Na<sub>2</sub>SO<sub>4</sub>. After removal the solvent under vacuum, the crude product obtained was purified by silica gel flash column chromatography (n-hexane/EtOAc 10:2) to generate the corresponding dibromo derivative (4, 6 or 8, respectively). For their spectral data and analyses (Figures S1-S6).



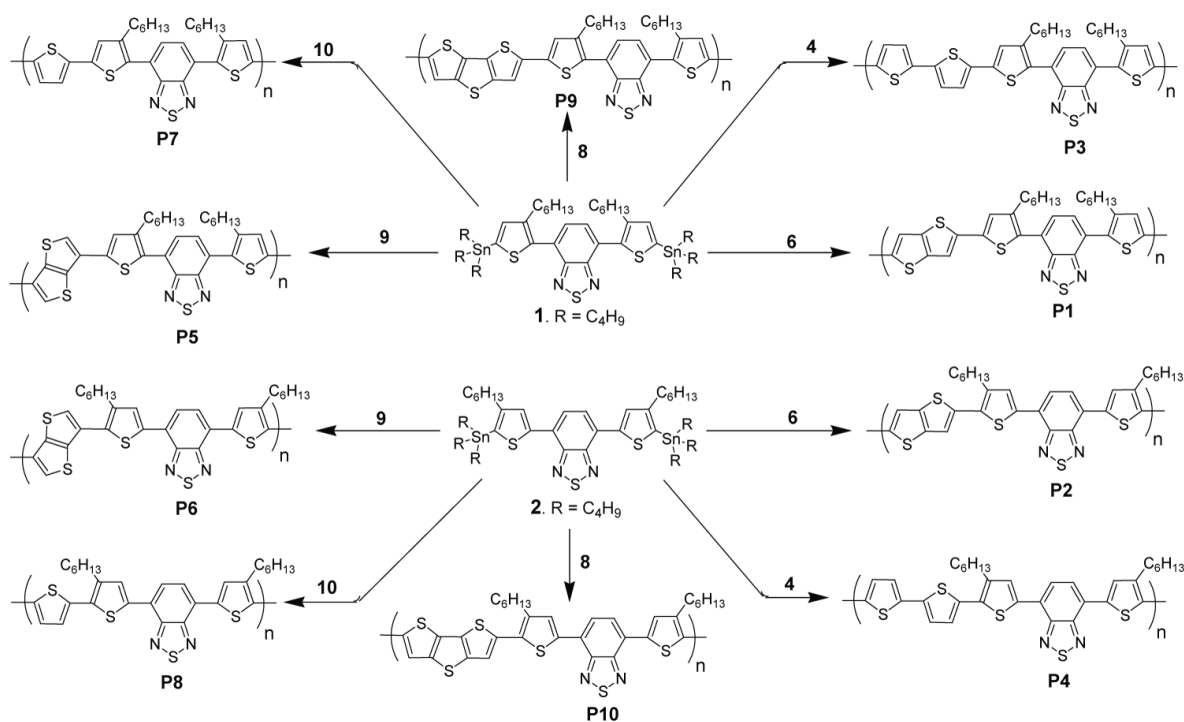
### General procedure for the microwave-assisted Stille cross-coupling polymerization

Equimolar amounts (0.5 mmol) from the desired dibromo and di(tributylstannyl) derivatives were dissolved in dry DMF and degassed with N<sub>2</sub> atmosphere for 30 min followed by adding Pd(PPh)<sub>4</sub>

(5 mol% relative to Br) and degassed again with nitrogen for 30 min. The screw capped glass tube was then irradiated by microwave under the following conditions: 5 min at 100°C, 5 min at 120°C and 30 min at 150°C. The end-capping process was performed in separated two steps: A solution of phenylboronic acid pinacol ester (5 mol%) in 0.5 mL DMF was first added, followed by irradiating the reaction mixture by microwave under the following condition: 2 min at 100°C, 2 min at 120°C and 5 min at 150°C. The same process was repeated by adding a solution of bromobenzene (5 mol%) in 0.5 mL DMF. The screw capped glass tube was allowed to return to room temperature and the reaction mixture was poured into methanol. The crude polymer was collected via filtration and washed successively with methanol. The residual solid was loaded into an extraction thimble and washed successively with methanol (24 h) followed by acetone (24 h). For the spectral data and analyses of copolymers P1-P10, see supporting information (Figures S7-S16).

## Results and Discussion

The two precursory comonomers 4,7-bis(5-tributylstannyl-3,3'/4,4'-hexylthiophene-2-yl)benzo[c][2,1,3]thiadiazoles 1 and 2, were readily synthesized in high yields according to our previously literature procedures [30]. Readily synthetic pathways were used for the synthesis of some donors as precursors (Scheme 1). Brominating 2,2'-bithiophene 3, thieno[3,2-b]thiophene 5 and/or dithieno[3,2-b;2,3'-d]thiophene 7 with NBS in THF at room temperature affording the corresponding dibromo derivatives 5,5'-dibromo-2,2'-bithiophene 4, 2,5-dibromothieno[3,2-b]thiophene 6 and 5,5'-dibromodithieno[3,2-b;2,3'-d]thiophene 8, respectively, in good yields. However, 3,6-dibromothieno[3,2-b]thiophene 9 and 2,5-dibromothiophene 10 were obtained from commercial sources.



**Scheme 2:** General pathways for the synthesis of  $\pi$ -conjugated copolymers P1-P10; Polymerization conditions: Stille cross-coupling: Pd(PPh<sub>3</sub>)<sub>4</sub>, DMF, microwave irradiation.

The title copolymers P1-P10 were prepared through Stille cross-coupling reaction between the proper brominated thiophene derivative and the proper distannyl derivative according to the synthetic routes depicted in Scheme 2. Stille cross-coupling of equimolar amounts of monomers 4, 6, 8, 9 or 10 with 4,7-bis(5-tributylstannyl-3,3'-hexylthiophene-2-yl)benzo[c][2,1,3]thiadiazole 1 afforded the corresponding copolymers P3, P1, P9, P5 and P7, respectively, in 75%-80% yields (Table 1).

Under the same reaction conditions, Stille cross-coupling of monomers 4, 6, 8, 9 or 10 with 4,7-bis(5-tributylstannyl-4,4'-hexylthiophene-2-yl)benzo[c][2,1,3]thiadiazole 2 afforded the corresponding copolymers P4, P2, P10, P6 and P8, respectively, in 60%-82% yields (Table 1).

All copolymers were precipitated into methanol and purified by Soxhlet extraction with methanol and acetone successively to remove residual catalyst, by-products and the lower molecular weight materials. They showed good solubility in most common organic solvents ( $>5 \text{ mg mL}^{-1}$ ), facilitating the different possible characterization including gel permeation chromatography (GPC), as well as the film-processing ability. The observed rather relatively lower  $M_n$  values of the resulting copolymers obtained from copolymerization of comonomer 2 compared to those obtained from copolymerization of comonomer 1, is probably due to the relatively steric hindrance effect resulting from the hexyl side chains at the 4,4'-positions in the thiophene rings of 2 (Table 1). However, in case of using comonomer 1, there should be much less steric hindrance effect in Stille coupling reaction. The <sup>1</sup>H NMR spectra for all polymers were found to be in

quite agreement with the proposed polymer structures (Figures S7-S16).

| Polymer | Mn                    | PDI                  | Yield            | Td                | Tg                |
|---------|-----------------------|----------------------|------------------|-------------------|-------------------|
|         | (kg/mol) <sup>b</sup> | (Mw/Mn) <sup>b</sup> | (%) <sup>c</sup> | (°C) <sup>d</sup> | (°C) <sup>e</sup> |
| P1      | 19.63                 | 1.54                 | 79.5             | 406.1             | 91.1              |
| P2      | 18.71                 | 1.49                 | 73.2             | 380.7             | 116.7             |
| P3      | 21.33                 | 1.63                 | 75.8             | 410.4             | 84.9              |
| P4      | 20.19                 | 1.45                 | 70.1             | 434.5             | 86.7              |
| P5      | 18.83                 | 1.69                 | 80               | 384.3             | 88.6              |
| P6      | 16.24                 | 1.55                 | 82               | 397.2             | 89.3              |
| P7      | 18.12                 | 1.71                 | 75               | 418.1             | 67.9              |
| P8      | 17.4                  | 1.66                 | 70               | 428.2             | 80.9              |
| P9      | 17.34                 | 1.76                 | 78.7             | 389.2             | 117.8             |
| P10     | 15.29                 | 1.59                 | 60               | 396.8             | 112.4             |

**Table 1:** Molecular and thermal properties of copolymers P1-P10<sup>a</sup>; <sup>a</sup>All polymerizations were carried out using Stille cross-coupling method in dry DMF in presence of Pd(PPh<sub>3</sub>)<sub>4</sub> under microwave irradiation; <sup>b</sup>Calculated from GPC (Eluent: CHCl<sub>3</sub>, polystyrene standards); <sup>c</sup>Based on the weight of polymer obtained after Soxhlet extraction and drying under vacuum; <sup>d</sup>Onset decomposition temperature (5% weight loss) measured by TGA under nitrogen atmosphere at a heating rate of 10°C/min; <sup>e</sup>Determined by DSC under nitrogen atmosphere at a heating rate of 10°C/min. The polymer samples were heated up to 300°C and the DSC reported data were obtained from the second heating cycle.

Thermogravimetric analysis (TGA) of copolymers P1-P10 revealed that the residual weights are all greater than 50% when the temperature rise to 800°C (Figure S17). Most of copolymers showed almost one step decomposition process and the thermal decomposition temperatures

(T<sub>d</sub>, 95 wt% residues) are in the range of 380.7°C-434.5°C (Table 1), indicative of high thermal stabilities, which could be ascribed to side chain decomposition upon heating processes [14,41]. Differential scanning calorimetry (DSC) of copolymers P1-P10 (Figure S18 and Table 1) revealed that the higher T<sub>g</sub> values are obtained from the polymers containing thieno[3,2-b]thiophene (connected at positions 2,5) and dithieno[3,2-b;2',3'-d]thiophene (91.12°C for P1), (116.7°C for P2), (117.8°C for P9), (112.4°C for P10), indicating highly ordered structures with strong intermolecular interactions in the latter copolymers. The other copolymers P3-P8 showed T<sub>g</sub> values in the range of 67.9°C~89.3°C. This owes to the stronger intermolecular interactions and the increasing interchain regularity caused by introducing fused ring aromatic moieties to copolymer main chains.

The theoretical calculations of the copolymers were calculated by density functional theory and time-dependent (DFT/TDDFT) quantum mechanical calculations at the level of B3LYP/6-311++G (d,p) [24,25,40]. The rigidity of copolymers can be attributed to the non-covalent S...N interactions, for example, in copolymer P10 the S...N distance is 2.89 Å, which is 14% less than the sum of Van der Waals radius. Not only rigidity, but also planarity of the copolymers affects the T<sub>g</sub> values. The planer copolymers such as P2, P4, P6, P8 and P10 having hexyl side chains at the 4,4'-positions in the thiophene rings of HT-BzT-HT unit showed higher T<sub>g</sub> values than their corresponding copolymers having hexyl side chains at the 3,3'-positions.

The DFT optimized structures of P1 and P2 are shown in Figure 1 as representative example and the rest were inserted in the supplementary information (Figure S19). The copolymers with the alkyl groups in the 2,5 positions have more planer structure than the copolymers with 3,3 position. For example, the dihedral angle C1-C2-C3-C4 and C5-C6-C7-C8 of P2 were 162° and 170° while those of P1 were 132° and 155°, respectively. However, good thermal stability of the copolymers prevents the deformation of the copolymers morphology and the degradation of the polymeric active layer under applied electric fields [41,42]. Thus, the synthesized copolymers might be considered as good candidates for several device applications.

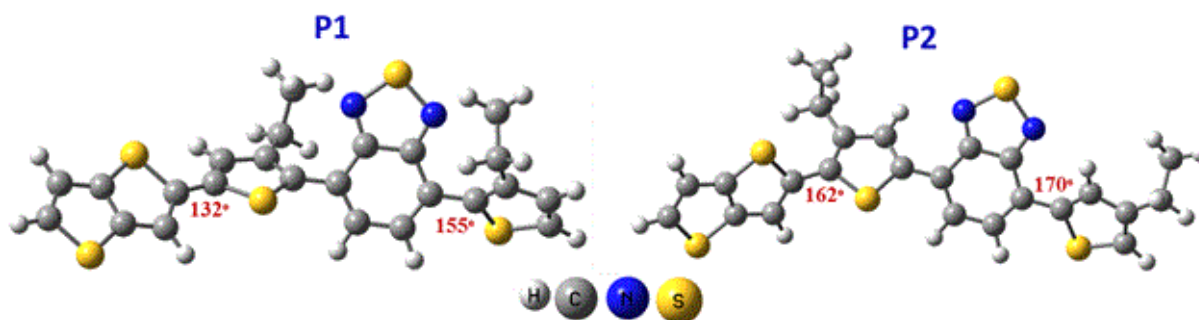


**Figure 1:** B3LYP/6-311++G (d,p) optimized structures of P1 and P2 copolymers as representative example.

The normalized optical absorption spectra of all copolymer solutions in chlorobenzene (CB) and as thin films casted from their CB solutions on glass slides are shown in Figure 2 and their spectral data are given in Table 2. It has been observed that the thin film absorption spectra for all polymers (Figures 2c and 2d) significantly broader and red-shifted than their corresponding absorption spectra in solutions

(Figures 2a and 2b) resulting in bathochromic shifts in absorption maximum, indicating increased backbone planarization and  $\pi$ -stacking in the solid states [42,43]. The aforementioned observation suggests that the molecules in the thin film underwent molecular organization to form more ordered structures. However, the long and

lower wavelength regions in the UV spectra of copolymers P1-P10 attributed to the ICT transition within the copolymer chains.

| Polymer | UV-Vis absorption     |                         |   |                       |                         |   | Cyclic voltammetry <sup>c</sup> |       |                              |
|---------|-----------------------|-------------------------|---|-----------------------|-------------------------|---|---------------------------------|-------|------------------------------|
|         | Solution              |                         |   | Film                  |                         |   | HOMO                            | LUMO  | E <sub>g</sub> <sup>ec</sup> |
|         | λ <sub>max</sub> (nm) | λ <sub>onset</sub> (nm) | E <sub>g</sub> <sup>opt</sup> (eV) <sup>b</sup> | λ <sub>max</sub> (nm) | λ <sub>onset</sub> (nm) | E <sub>g</sub> <sup>opt</sup> (eV) <sup>b</sup> | (eV)                            | (eV)  | (eV)                         |
| P1      | 501                   | 593                     | 2.09  | 532                   | 674                     | 1.83  | -5.27                           | -3.25 | 2.02                         |
| P2      | 530                   | 639                     | 1.78  | 557                   | 705                     | 1.75  | -5.18                           | -3.43 | 1.75                         |
| P3      | 500                   | 595                     | 2.08  | 525                   | 657                     | 1.88  | -5.40                           | -3.46 | 1.94                         |
| P4      | 540                   | 642                     | 1.93  | 565                   | 697                     | 1.77  | -5.31                           | -3.53 | 1.78                         |
| P5      | 469                   | 558                     | 2.22  | 481                   | 613                     | 2.02  | -5.60                           | -3.40 | 2.2                          |
| P6      | 504                   | 584                     | 2.12  | 515                   | 623                     | 1.99  | -5.41                           | -3.35 | 2.06                         |
| P7      | 503                   | 591                     | 2.09  | 517                   | 632                     | 1.96  | -5.39                           | -3.40 | 1.99                         |
| P8      | 547                   | 652                     | 1.9   | 597                   | 743                     | 1.66  | -5.22                           | -3.45 | 1.77                         |
| P9      | 500                   | 594                     | 2.08  | 525                   | 681                     | 2.82  | -5.26                           | -3.31 | 1.95                         |
| P10     | 538                   | 639                     | 1.94  | 574                   | 758                     | 1.63  | -5.19                           | -3.40 | 1.79                         |

**Table 2:** Optical and electrochemical characterizations of copolymers P1-P10<sup>a</sup>; <sup>a</sup>All data are for those copolymers prepared by microwave polymerization reaction conditions; <sup>b</sup>Optical band gap (E<sub>g</sub><sup>opt</sup>) was calculated from the intersection of the tangent on the low energetic edge of the absorption spectrum with the baseline; <sup>c</sup>The onset potentials are obtained from the intersection of the two tangents down at the rising current and the baseline changing current of the CV curves.

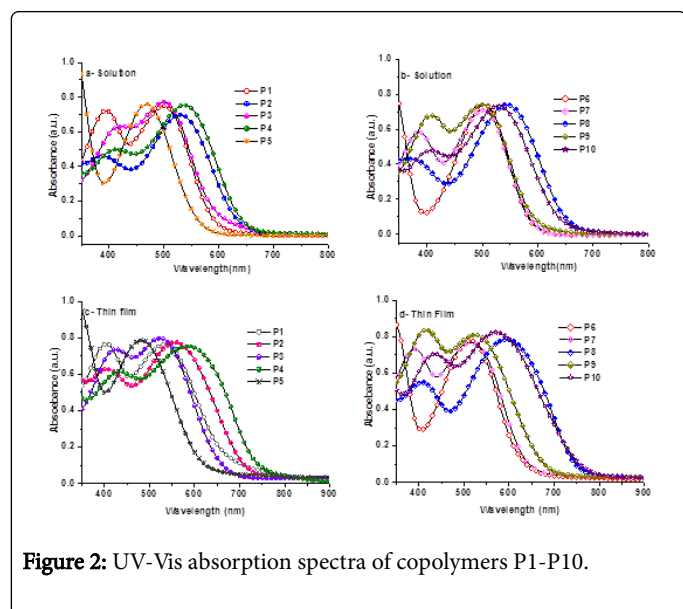


**Figure 2:** UV-Vis absorption spectra of copolymers P1-P10.

Figure 3 showed the measured and computed UV-Vis spectra of P9 and P10 as representative example. Good agreements were obtained between the measured absorption maximum and the computed one. For example, the measured and computed absorption maxima of P9 and P10 were 500 nm, 501 nm and 538 nm, 550 nm, respectively. Upon investigation of the molecular orbitals that involved in these electronic transitions we found that HOMO-LUMO electronic transition was the main route. Evidently the ICT can be seen from molecular orbital

tology as shown in Figure 3. The HOMO was delocalized over molecular skeleton of P9 or P10, while the LUMOs were mainly localized on the acceptor moiety. This indicates that ICT was originated mainly from the donor unit (thiophene units) to transfer to the acceptor unit (benzothiadiazole unit) upon excitation.

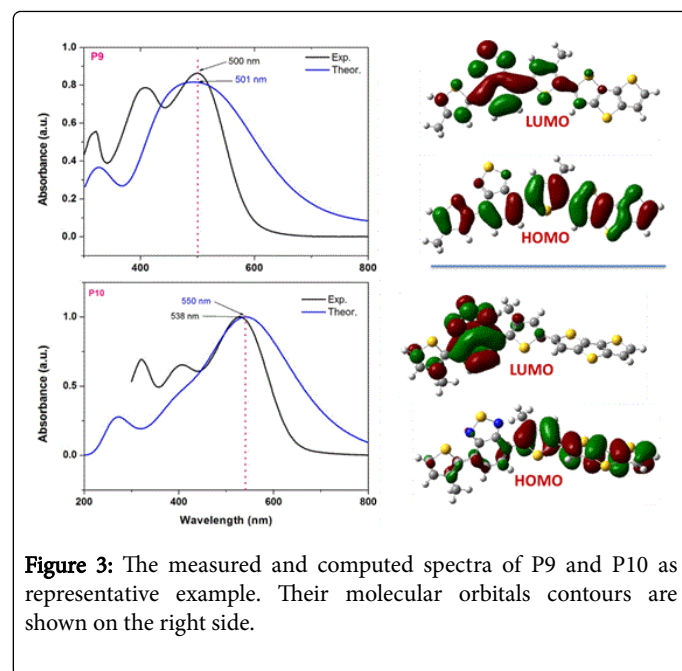


**Figure 3:** The measured and computed spectra of P9 and P10 as representative example. Their molecular orbitals contours are shown on the right side.

In the case of copolymer P10, the absorption onset in CB solution was at 639 nm, which is ~119 nm blue-shifted compared to its thin film absorption onset (at 758 nm), indicating increased planarization (the dihedral angle close to 180°, Figure 3) and improved  $\pi$ -stacking in the solid state. Based on their onset absorption wavelengths, the optical band gaps of all polymers were reduced to significant lower values in solid state (Table 2). It is worth mentioning that the stabilization of quinoidal structure in copolymer P10 containing dithieno[3,2-b;2,3'-d]thiophene moiety results in a low band gap of about 1.63 eV, showing efficient absorption around the region with the highest photon flux of the solar spectrum (about 758 nm). Besides, the DFT calculations showed that P10 had the lowest energy gap (2.17 eV) in the gas phase.

TDDFT calculations based on the optimized structures of the individual substituent units (Figure 4) have energy gap in the order T>TT>BT>DTT, as a result of decreasing the energy values of both the HOMO and LUMO in the same order. Hence, when the substituents attached to the polymers backbone, the average HOMO and LUMO of the copolymers decreases accordingly. Both theoretical and experimental results indicate that the fused ring aromatic structures, in particular P10 that contains DTT unit, have a strong tendency to form  $\pi$ - $\pi$  stacks with a large overlapping area that is preferable for charge carrier transport through intermolecular hopping, and to induce a higher order molecular organization that leads to large crystalline domains and less disordered domain boundaries [21,44,45].

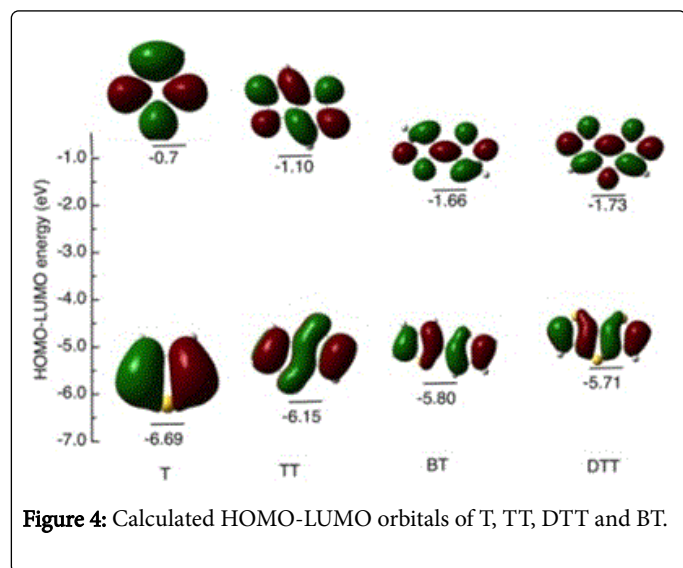


Figure 4: Calculated HOMO-LUMO orbitals of T, TT, DTT and BT.

The aforementioned results suggest that incorporating dithieno[3,2-b;2,3'-d]thiophene, thiophene, thieno[3,2-b]thiophene (connected at positions 2,5) and 2,2'-bithiophene moieties within the polymer chains extends the absorption of copolymers P2, P4, P8 and P10 and creates an optical band gap that is much smaller than any of the other polymers. However, moving the hexyl chains from 3,3'- to 4,4'-positions increases the planarity in the thiophene rings of the resulting copolymers and produces a positive shift for each of the maximum and edge absorptions [31]. Thus, the red-shift might be attributed to the high co-planar confirmation of adjacent thiophene rings induced by the hexyl side chains at the 4,4'-positions on the thiophene rings in the polymer backbone that increase the effective conjugation length. Similar behaviors were observed in the UV-Vis absorption spectra of similar polymers [14,21,46].

The oxidation and reduction potentials of copolymers P1-P10 were determined by cyclic voltammetry (CV) (Figure S20). The electrochemical results are summarized in Table 2. As shown in Figure S20, All copolymers are electrochemically active and undergo a quasi-reversible redox reaction. The estimated HOMO and LUMO energy levels were found to be in the range of -5.02 to -5.63 eV and -3.29 to -3.53 eV, respectively. Most of the HOMO energy levels were found to be below the air oxidation threshold (ca. -5.27 eV) which revealed that they may show good stabilities toward air and oxygen (a prerequisite when considering device application) [47]. Moreover, their LUMO energy levels with regard to that of PCBM (-4.2 eV) are adequate for exciton dissociation [14,48]. However, in some cases, the  $E_g^{ec}$  of polymers was found to be somewhat higher than of  $E_g^{opt}$ . This is might be originated from the interface barrier present between the polymer film and the electrode surface [39,46,47]. As shown by the UV-Vis absorption spectra as well as their CV data (Table 2), not only changing the position of hexyl side chains on the thiophene rings but also incorporating different donor moieties in the polymer chains exert marked effects on the photo- and electrochemical behaviours.

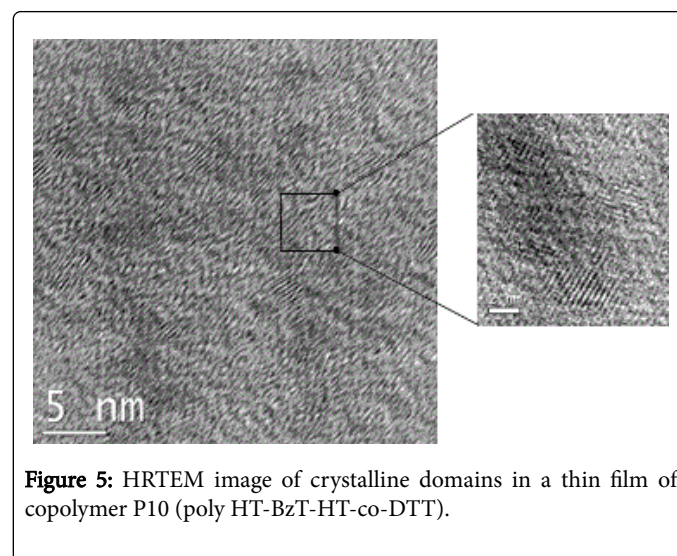


Figure 5: HRTEM image of crystalline domains in a thin film of copolymer P10 (poly HT-BzT-HT-co-DTT).

Since the solid state morphology and molecular organization of the polymer greatly impacts the overall performance of bulk heterojunction solar cells, we examined the morphology of the best performing polymer, P10 (poly HT-BzT-HT-co-DTT), via X-ray diffractometry (XRD) and transmittance electron microscopy (TEM) measurements. XRD measurement of a polymer thin film revealed that this polymer formed a crystalline structure in the thin film with an interlayer lamellar d100-spacing of 13.21 Å ( $2\theta=6.68^\circ$ ; Figure S21). Another diffraction peaks are observed at  $2\theta=11.34^\circ$  (200) and  $2\theta=16.26^\circ$  (300), indicating a high degree of crystallinity in copolymer P10 thin film. The observed interlayer distance is much shorter than the calculated width of the fully extended polymer chain (~36 Å), indicating that the side chains are either bent [49] or interdigitated with the side chains in adjacent layers [50]. The small  $\pi$ - $\pi$  stacking distance (3.86 Å) between polymer backbones suggested that there are strong intermolecular interaction forces that can be accounted for by the  $\pi$ - $\pi$  stacking of fused ring moieties (DTT and BzT) and the donor-acceptor interaction of DTT (and the thiophene units) with BzT in this polymer [51]. The high-resolution transmission electron microscopy (HRTEM) of the polymer: PC60BM blend image shown in Figure 5 clearly shows the crystal lattices of a thin film of P10 (PHT-BzT-HT-

co-DTT) domains, where the (020) fringes have a d-spacing of 3.86 Å, corresponding to the face-to-face  $\pi$ - $\pi$  stacking distance.

Photovoltaic devices of copolymers P2, P4, P6, P8 and P10 with a configuration of ITO/PEDOT: PSS/active layer/Al were fabricated and the active layer was a blend of copolymers P2, P4, P6, P8 and P10 with PC<sub>60</sub>BM spin coated from their CB solutions to achieve reasonable film thickness (~100 nm) for the fabrication of BHJ devices. The donor/acceptor ratio was optimized and found to be 1/1 (wt./wt.) for all polymers. The BHJ solar cells data, including the short circuit current density (J<sub>sc</sub>), the open circuit-voltage (V<sub>oc</sub>), the fill factor (FF), and the power conversion efficiency (PCE) of copolymers P2, P4, P6, P8 and P10 are summarized in Table 3. The photovoltaic parameters of copolymer P10 are shown in Figure 6.

| Polymer | Thickness (nm) | Voc (V) | Jsc (mA/cm <sup>2</sup> ) | FF (%) | h (%) | Rs (Ω/cm <sup>2</sup> ) |
|---------|----------------|---------|---------------------------|--------|-------|-------------------------|
| P2      | 95             | 0.53    | 4.45                      | 66     | 1.53  | 39                      |
| P4      | 97             | 0.52    | 4.44                      | 64     | 1.5   | 37                      |
| P6      | 100            | 0.53    | 3.96                      | 65     | 1.35  | 40                      |
| P8      | 101            | 0.53    | 5.45                      | 63     | 1.81  | 42                      |
| P10     | 99             | 0.53    | 5.68                      | 64     | 1.91  | 38                      |

**Table 3:** Characteristic parameters of photovoltaic cells based on copolymers P2, P4, P6, P8, and P10 with PC<sub>60</sub>BM<sup>a</sup>; <sup>a</sup> In all cases, polymer:PC<sub>60</sub>BM ratio was 1:1.

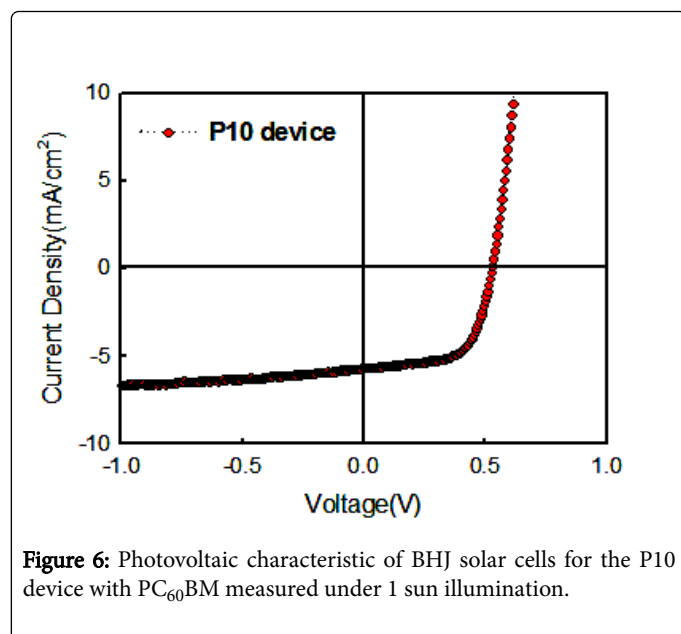


**Figure 6:** Photovoltaic characteristic of BHJ solar cells for the P10 device with PC<sub>60</sub>BM measured under 1 sun illumination.

According to the presented data, all devices with the different donor materials showed the same V<sub>oc</sub> of 0.53 V, however, the most effective parameter on the efficiency was J<sub>sc</sub> device based copolymers P2 and P4 showed almost characteristic parameters of photovoltaic cells. The effect of twisted backbone shape on the J<sub>sc</sub> can be seen by comparing device based P2 with device based P6. Both copolymers have same thieno[3,2-b]thiophene moiety in different connection position. In case of copolymer P6 (connected at positions 3,6), thienothiophene unit twisted along the polymer structure which leads to decreasing

extent of  $\pi$ - $\pi$  orbital overlap and planarity. These morphological properties caused blue shift in the spectral area and lower crystallinity compare to P2 film.

As shown in Figure 2, due to blue shifted spectral area within the solar spectrum, the number of photo-generated carriers in P6 polymer thin film was decreased. The total area percentage of absorption spectrum decrement of P6 polymer film compared with the P2 polymer film was nearby 30% which led to the decrement of the J<sub>sc</sub> value. Numerical quantitative comparison between absorption area change and J<sub>sc</sub> value is not matching due to the side effects (e.g. refractive index, exciton generation position, etc.). Also, the lower FF due to the lower planarity in copolymer P6 compared to P2 could be another reason for lower efficiency. To obtain high FF organic solar cells, the device should have small R<sub>s</sub> value which is the value interpret the efficient charge transport characteristic inside the device with highly crystallized film based better  $\pi$ -stacking property [15,21,52]. The twisted shaped P6 backbone gave adverse effect on the crystallinity which led to higher series resistance of P6 based device (40 Ω/cm<sup>2</sup>) than P2 based device (38 Ω/cm<sup>2</sup>).

The effect of used ring structures with different number of thiophene ring in the polymer backbone can be seen by comparing device based P8 (thiophene), P2 (thieno[3,2-b]thiophene) and P10 (dithieno[3,2-b;2',3'-d]thiophene). For each device, the V<sub>oc</sub> was not affected as the number of thiophene ring increased, while R<sub>s</sub> were found to decrease. This conspicuous decrease is probably due to the better mobility in the longer fused ring backbone. Finally, device based P10 with dithieno[3,2-b;2',3'-d]thiophene moiety show the highest photovoltaic performances with PCE of 1.91% and J<sub>sc</sub> of 5.67 mA/cm<sup>2</sup>. It is noteworthy to mention that solar cell based P2 polymer shows lower PCE due to the lower J<sub>sc</sub> than device based P8 polymer even though better FF with lower R<sub>s</sub>. It can be explained with reduced number of photo-generated carriers in P2 polymer film due to blue shifted spectral area compare to the P8 polymer. Considering the relatively narrow absorption bands of the copolymers P2, P4, P6, P8 and P10:PC<sub>60</sub>BM blends and unoptimized nature of the BHJ solar cells with respect to blend composition, active layer film thickness and molecular weight, we conclude that benzothiadiazole-thiophenes copolymers semiconductors are promising for photovoltaic cell.

## Conclusion

Donor/Acceptor  $\pi$ -conjugated copolymers based on comonomers HT-BzT-HT incorporating with various donating units possessed low band gap were readily prepared via the Stille cross-coupling reaction, under microwave irradiation, in good yields with good solubilities in most common organic solvents and excellent film-processing ability. The use of fused ring structures such as DTT and TT units could enhance the conjugation, planarity, and interchain interaction. Moreover, the planarity, enhanced conjugation and possible S-S interaction make DTT and TT a very useful building block for organic electronic materials. Incorporating DTT within the polymer chains extends the absorption onset beyond 758 nm and creates an optical band gap that is much smaller than any of the other polymers. In view of their original electronic properties, the synthesized polymers could lead to interesting active materials for the realization of electronic devices. The device performance was achieved by simply fabricated devices without additives or extra layers, which facilitate the preparation of low cost polymer solar cells. The highest PCE (1.91%) was achieved from P10/PC<sub>60</sub>BM among the synthesized copolymers and all data are obtained by simply fabricated devices without additives

or extra layers. We are currently focusing on synthesizing new derivatives such kinds of polymers in order to improve the performance in photovoltaic cells.

## Acknowledgement

This work was financially supported by the Science & Technology Development Fund (STDF) (Egypt) through the STDF-NRG Project – ID Project Number: 7973. This work was also supported by the GIST Research Institute (GRI) in 2018. El-Shehawey A. would like also to acknowledge the generous support from Kafrelsheikh University Research Program (ID: KFSU-3-13-04).

Additional Supporting Information found in the online version of this article.

## References

- Po R, Roncali J (2016) Beyond efficiency: Scalability of molecular donor materials for organic photovoltaic. *J Mater Chem C* 4: 3677-3685.
- An Q, Zhang F, Zhang J, Tang W (2016) Versatile ternary organic solar cells: A critical review. *Energy Environ Sci* 9: 281-322.
- Facchetti A (2011)  $\pi$ -Conjugated polymers for organic electronics and photovoltaic cell applications. *Chem Mater* 23: 733-758.
- Zhou H, Yang L, You W (2012) Rational design of high performance conjugated polymers for organic solar cells. *Macromolecules* 45: 607-632.
- Yin Z, Wei J, Zheng Q (2016) Interfacial materials for organic solar cells: Recent advances and perspectives. *Adv Sci* 3: 1500362.
- Cheng YJ, Yang SH, Hsu CS (2009) Synthesis of conjugated polymers for organic solar cell applications. *Chem Rev* 109: 5868-5923.
- Zhang Z-G, Wang J (2012) Structures and properties of conjugated donor-acceptor copolymers for solar cell applications. *J Mater Chem* 22: 4178-4187.
- Jiang JM, Yuan MC, Dinakaran K, Hariharanb A, Wei K-H (2013) Crystalline donor-acceptor conjugated polymers for bulk heterojunction photovoltaics. *J Mater Chem A* 1: 4415-4422.
- Jung JW, Jo JW, Jung EH, Jo WH (2016) Recent progress in high efficiency polymer solar cells by rational design and energy level tuning of low band gap copolymers with various electron-withdrawing units. *Org Electron* 31: 149-170.
- Dennler G, Scharber MC, Ameri T, Denk P, Forberich K, et al. (2008) Design rules for donors in bulk heterojunction tandem solar cells towards 15% energy conversion efficiency. *Adv Mater* 20: 579-583.
- Cai W, Gong X, Cao Y (2010) Polymer solar cells: Recent development and possible routes for improvement in the performance. *Sol Energy Mater Sol Cells* 94: 114-127.
- Beaujuge PM, Amb CM, Reynolds JR (2010) Spectral engineering in  $\pi$ -conjugated polymers with intramolecular donor-acceptor interactions. *Acc Chem Res* 43: 1396-1407.
- Gibson GL, McCormick TM, Seferos DS (2012) Atomistic band gap engineering in donor-acceptor polymers. *J Am Chem Soc* 134: 539-547.
- Scharber MC, Mühlbacher D, Koppe M, Denk P, Waldauf C, et al. (2006) Design rules for donors in bulk-heterojunction solar cells-Towards 10% energy-conversion efficiency. *Adv Mater* 18: 789-794.
- Singh RP, Kushwaha OS (2017) Progress towards efficiency of polymer solar cells. *Adv Mater Lett* 8: 2-7.
- Dou L, You J, Hong Z, Xu Z, Li G, et al. (2013) 25<sup>th</sup> anniversary article: A decade of organic/polymeric photovoltaic research. *Adv Mater* 25: 6642-6671.
- Peng Q, Liu XJ, Su D, Fu GW, Xu J, et al. (2011) Novel benzo[1,2-b:4,5-b']dithiophene-benzothiadiazole derivatives with variable side chains for high-performance solar cells. *Adv Mater* 23: 4554-4558.
- You J, Dou L, Yoshimura K, Kato T, Ohya K, et al. (2013) A polymer tandem solar cell with 10.6% power conversion efficiency. *Nat Commun* 4: 1446-1456.
- Li Z, Lin H, Jiang K, Carpenter J, Li Y, et al. (2015) Dramatic performance enhancement for large band gap thick-film polymer solar cells introduced by a difluorinated donor unit. *Nano Energy* 15: 607-615.
- Bin H, Gao L, Zhang ZG, Yang Y, Zhang Y, et al. (2016) 11.4% Efficiency non-fullerene polymer solar cells with trialkylsilyl substituted 2D-conjugated polymer as donor. *Nat Commun* 7: 13651.
- Chochos CL, Choulis SA (2011) How the structural deviations on the backbone of conjugated polymers influence their optoelectronic properties and photovoltaic performance. *Prog Polym Sci* 36: 1326-1414.
- Peng Q, Liang T, Feng K (2013) Design of low band gap conjugated polymers for organic solar cell application. *Mater Processes Energy Curr Res Dev* 1:11-21.
- Kim Y, Lim E (2014) Development of polymer acceptors for organic photovoltaic cells. *Polymers* 6: 382-407.
- Frisch MJ, Trucks GW, Schlegel HB, Scuseria GE, Robb MA, et al. (2010) Electronic supplementary material for chemical science. *RSC Adv* 1: 10-15.
- McCormick TM, Bridges CR, Carrera EI, DiCarmine PM, Gibson GL, et al. (2013) Conjugated polymers: Evaluating DFT methods for more accurate orbital energy modeling. *Macromolecules* 46: 3879-3886.
- Zhao X, Lv H, Yang D, Li Z, Chen Z, et al. (2015) A novel crystallizable low band gap polymer for high-efficiency polymer photovoltaic cells. *J Polym Sci Part A Polym Chem* 54: 44-48.
- Li Z, Zhang T, Xin Y, Zhao X, Yang D, et al. (2016) Synergistic effect of fluorination and regioregularity on the long-term thermal stability of polymer solar cells. *J Mater Chem A* 4: 18598-18606.
- Cao Y, Lei T, Yuan J, Wang J-Y, Pei J (2013) Dithiazolyl-benzothiadiazole-containing polymer acceptors: Synthesis, characterization and all-polymer solar cells. *Polym Chem* 4: 5228-5236.
- Li Y, Pan Z, Miao L, Xing Y, Lia C, et al. (2014) Fluoro-benzoselenadiazole-based low band gap polymers for high efficiency organic solar cells. *Polym Chem* 5: 330-334.
- El-Shehawey AA, Abdo NI, El-Barbary AA, Lee JS (2011) Alternating copolymers based on 2,1,3-benzothiadiazole and hexylthiophene: Positioning effect of hexyl chains on the photophysical and electrochemical properties. *Eur J Org Chem* 4841-4852.
- Abdo NI, Ku J, El-Shehawey AA, Shim HS, Min JK, et al. (2013) Synthesis and characterization of low band gap  $\pi$ -conjugated copolymers incorporating 4,7-bis(3,3'/4,4'-hexylthiophene-2-yl)benzo[c][2,1,3]thiadiazole units for photovoltaic application. *J Mater Chem A* 1: 10306-10317.
- Abdo NI, El-Shehawey AA, El-Barbary AA, Lee JS (2012) Palladium-catalyzed direct C-H arylation of thieno[3,4-b]pyrazines: Synthesis of advanced oligomeric and polymeric materials. *Eur J Org Chem*, pp: 5540-5551.
- Elsawy W, Lee CL, Cho S, Oh SH, Moon SH, et al. (2013) Isoindigo-based small molecules for high-performance solution-processed organic photovoltaic devices: The electron donating effect of the donor group on photo-physical properties and device performance. *Phys Chem Chem Phys* 15: 15193-15203.
- Elsawy W, Kang H, Yu K, Elbarbary A, Lee K, et al. (2014) Synthesis and characterization of isoindigo-based polymers using CH-arylation polycondensation reactions for organic photovoltaics. *J Polym Sci A Polym Chem* 52: 2926-2933.
- Elsawy W, Son M, Jang J, Kim MJ, Ji Y, et al. (2015) Isoindigo-based donor-acceptor conjugated polymers for air-stable non-volatile memory devices. *ACS Macro Lett* 4: 322-326.
- Shaker M, Lee J-H, Trinh CK, Kim W, Lee K, et al. (2015) A facile method to synthesize [A'(D'AD)]<sub>2</sub>-based push-pull small molecules for organic photovoltaics. *RSC Adv* 5: 66005-66012.
- Shaker M, Trinh CK, Kim W, Kim H, Lee K, et al. (2015) Direct C-H arylation synthesis of (DD'AD'DA')-constituted alternating polymers

- with low band gaps and their photovoltaic performance. *New J Chem* 39: 4957-4964.
38. Li Y, Cao Y, Gao J, Wang D, Yu G, et al. (1999) Electrochemical properties of luminescent polymers and polymer light-emitting electrochemical cells. *Synth Met* 99: 243-248.
39. Wang E, Wang M, Wang L, Duan C, Zhang J, et al. (2009) Donor polymers containing benzothiadiazole and four thiophene rings in their repeating units with improved photovoltaic performance. *Macromolecules* 42: 4410-4415.
40. Frisch MJ, Trucks GW, Schlegel HB, Scuseria GE, Robb MA, et al. (2009) Gaussian 09, Gaussian, Inc. Wallingford CT.
41. Zhang T, Wu X, Luo T (2014) Polymer nanofibers with outstanding thermal conductivity and thermal stability: Fundamental linkage between molecular characteristics and macroscopic thermal properties. *J Phys Chem C* 118: 21148-21159.
42. Tessarolo M, Guerrero A, Gedefaw D, Bolognesi M, Prosa M, et al. (2015) Predicting thermal stability of organic solar cells through an easy and fast capacitance measurement. *Sol Ener Mater Sol Cells* 141: 240-247.
43. Kokubo H, Sato T, Yamamoto T (2006) Synthesis of new thiophene-based  $\pi$ -conjugated polymers for investigation of molecular alignment on the surface of platinum plate. *Macromolecules* 39: 3959-3963.
44. McCulloch I, Heeney M, Bailey C, Genevicius K, Macdonald I, et al. (2006) Liquid-crystalline semiconducting polymers with high charge-carrier mobility. *Nat Mater* 5: 328-333.
45. Pan H, Li Y, Wu Y, Liu P, Ong BS, et al. (2007) Low-temperature, solution-processed, high-mobility polymer semiconductors for thin-film transistors. *J Am Chem Soc* 129: 4112-4113.
46. DaSilva DJ, Takimoto HG, WeberdosSantos KCC, Garcia JR, Balogh DT, et al. (2016) Effect of hexyl substituent groups on photophysical and electrochemical properties of the poly[(9,9-dioctylfluorene)-2,7-diyl-alt-(4,7-bis(3-hexylthien-5-Yl)-2,1,3-benzothiadiazole)-2',2"-diyl]. *J Polym Sci B Polym Phys* 54: 1975-1982.
47. Park SH, Roy A, Beaupre S, Cho S, Coates N, et al. (2009) Bulk heterojunction solar cells with internal quantum efficiency approaching 100%. *Nat Photon* 3: 297-303.
48. Blom PWM, Mihailetchi VD, Koster JA, Markov DE (2007) Device physics of polymer: fullerene bulk heterojunction solar cell. *Adv Mater* 19: 1551-1556.
49. Pan H, Liu P, Li Y, Wu Y, Ong BS, et al. (2007) Unique polymorphism of oligothiophenes. *Adv Mater* 19: 3240-3243.
50. Ong BS, Wu Y, Liu P (2004) High-performance semiconducting polythiophenes for organic thin-film transistors. *J Am Chem Soc* 126: 3378-3379.
51. Osaka I, Sauv e G, Zhang R, Kowalewski T, McCullough RD (2007) Novel thiophene-thiazolothiazole copolymers for organic field-effect transistors. *Adv Mater* 19: 4160-4165.
52. Jao MH, Liao HC, Su WF (2016) Achieving a high fill factor for organic solar cells. *J Mater Chem A* 4: 5784-5801.